

# Modelling tidal stream turbines in a three-dimensional wave-current fully coupled oceanographic model



Xiaorong Li <sup>a</sup>, Ming Li <sup>b,\*</sup>, Stuart J. McLelland <sup>c</sup>, Laura-Beth Jordan <sup>c</sup>, Stephen M. Simmons <sup>c</sup>, Laurent O. Amoudry <sup>d</sup>, Rafael Ramirez-Mendoza <sup>d,e</sup>, Peter D. Thorne <sup>d</sup>

<sup>a</sup> School of Environmental Sciences, University of Liverpool, Liverpool, L69 7ZT, UK

<sup>b</sup> School of Engineering, University of Liverpool, Liverpool, L69 3GQ, UK

<sup>c</sup> School of Environmental Sciences, University of Hull, Cottingham Road, Hull, HU6 7RX, UK

<sup>d</sup> National Oceanography Centre, Joseph Proudman Building, 6 Brownlow Street, Liverpool, L3 5DA, UK

<sup>e</sup> CICESE, Carretera Ensenada-Tijuana No. 3918, Zona Playitas, Ensenada, B.C., 22860, Mexico

## ARTICLE INFO

### Article history:

Received 1 October 2016

Received in revised form

11 February 2017

Accepted 13 February 2017

Available online 20 February 2017

### Keywords:

Tidal stream energy

Three-dimensional

Oceanographic model

## ABSTRACT

A tidal turbine simulation system is developed based on a three-dimensional oceanographic numerical model. Both the current and turbulent controlling equations are modified to account for impact of tidal turbines on water velocity and turbulence generation and dissipation. High resolution mesh size at the turbine location is assigned in order to capture the details of hydrodynamics due to the turbine operation. The system is tested against comprehensive measurements in a water flume experiment and results of Computational Fluid Dynamics (CFD) simulations. The validation results suggest that the new modelling system is proven to be able to accurately simulate hydrodynamics with the presence of turbines. The developed turbine simulation system is then applied to a series of test cases in which a standalone turbine is deployed. Here, complete velocity profiles and mixing are realized that could not have been produced in a standard two-dimensional treatment. Of particular interest in these cases is an observed accelerated flow near the bed in the wake of the turbine, leading to enhanced bottom shear stress ( $\sim 2 \text{ N/m}^2$  corresponding to the critical stress of a range of fine gravel and finer sediment particles).

© 2017 The Author(s). Published by Elsevier Ltd. This is an open access article under the CC BY license (<http://creativecommons.org/licenses/by/4.0/>).

## 1. Introduction

As a response to the natural energy resource shortage and worldwide climate change, due in part to burning of fossil fuels to fulfil ever growing energy requirements, clean and renewable alternatives have been gaining significant attention. For example, the UK is aiming for 15% of the country's total energy production to be produced from renewable resources by 2020 [1]. In this regard, tidal stream energy is considered to be a very promising avenue of investigation due to its consistent predictability and availability. At the time of writing, 119 Tidal Energy Converter (TEC) concepts, developed by different companies, are listed on the European Marine Energy Centre (EMEC)'s website<sup>1</sup>; with full-scale tests of such devices currently underway in coastal waters around the world.

However, despite the growing interest in tidal stream energy exploitation, the analysis of the turbine-induced environmental impact has yet to be a primary focus of any major on-site TEC project, leaving large gaps in our understanding of the impacts of tidal stream energy devices. Alternatively, prototype experiments and numerical models are widely used to investigate such impacts. Prototype experiments often involve small scale laboratory studies, for example [2–4], used porous discs to simulate turbines in basic experiments, and more recently, in an effort to reproduce turbulent effects induced by real turbines, down-scaled dynamic turbine prototype models have been considered [5,6]. As a complement to practical laboratory prototype experiments, Computational Fluid Dynamics (CFD) modelling is another common way to study turbine behaviours. Similar to practical experiments, earlier studies conducted using CFD software packages approximated turbines as porous discs [7–9]. Works with realistic turbine geometry resolved in the calculating mesh have been published very recently [10–12]. These studies focus on how flow patterns are changed both upstream and downstream of the turbine in near-field scale, and in

\* Corresponding author.

E-mail addresses: [xiaorong.li@liverpool.ac.uk](mailto:xiaorong.li@liverpool.ac.uk) (X. Li), [mingli@liverpool.ac.uk](mailto:mingli@liverpool.ac.uk) (M. Li).

<sup>1</sup> <http://www.emec.org.uk/marine-energy/tidal-developers/>.

Nomenclature			
$\%_{RMSE}$	% Root Mean Square Error	$P_l$	The turbine-induced interference for the turbulence length-scale (l)
$\kappa$	The von Karman constant	$P_{td}$	The turbine-induced turbulence dissipation term
$\rho_0$	The water density	$P_{tp}$	The turbine-induced turbulence generation term
$\tau_{bx}$	The bottom stress in the $x$ direction	$q$	The non-hydrostatic pressure
$\tau_{by}$	The bottom stress in the $y$ direction	$q^2$	The turbulent kinetic energy
$\tau_{sx}$	The surface wind stress in the $x$ direction	$q_i$	One record in the validation data
$\tau_{sy}$	The surface wind stress in the $y$ direction	$q_{iest}$	One record in the calculated result
$\bar{W}$	The wall proximity function	$q_{max}$	The maximum record in the calculated result
$\varepsilon$	The turbulent kinetic energy dissipation rate	$q_{min}$	The minimum record in the calculated result
$\vec{V}$	The flow velocity vector	$S_h$	A stability function
$\zeta$	The height of the free surface	$S_m$	A stability function
$B_1$	A model coefficient $B_1 = 16.60$	$t$	Time
$C_d$	The drag coefficient	$u$	The velocity component in the $x$ direction
$C_{ext}$	The energy extraction coefficient	$u_{rb}$	The water friction velocity associated with the bottom
$C_l$	The coefficient of term $P_l$	$u_{rs}$	The water friction velocity associated with the surface
$C_{td}$	The coefficient of term $P_{td}$	$v$	The velocity component in the $y$ direction
$C_{tp}$	The coefficient of term $P_{tp}$	$w$	The velocity component in the $z$ direction
$D$	The diameter of the turbine	$x$	The east axis in the Cartesian coordinate system
$d$	The total water column depth	$y$	The north axis in the Cartesian coordinate system
$E$	The evaporation	$z$	The vertical axis in the Cartesian coordinate system
$E_1$	A model coefficient $E_1 = 1.80$	$z_0$	The bottom roughness parameter
$E_2$	A model coefficient $E_2 = 1.33$	$z_{ab}$	The reference height
$f$	The Coriolis parameter	CFD	Computational Fluid Dynamics
$F_l$	The horizontal diffusion of the macroscale	EMEC	European Marine Energy Centre
$F_q$	The horizontal diffusion of the turbulent kinetic energy	FVCOM	The Unstructured Grid Finite Volume Community Ocean Model
$F_u$	The horizontal momentum term in the $x$ direction	HATT	Horizontal Axis Tidal Turbine
$F_v$	The horizontal momentum term in the $y$ direction	ROMS	Regional Ocean Modelling System
$H$	The bottom depth	TbM	Current-only FVCOM case with turbulence terms activated at the turbine location (for model validation)
$K_m$	The vertical eddy viscosity coefficient	TbM15	Current-only FVCOM case with turbulence terms activated at the turbine location (for impact identification)
$K_q$	The vertical eddy diffusion coefficient of the turbulent kinetic energy	TbO	Current-only FVCOM case without turbulence terms (for model validation)
$l$	The macroscale	TbO15	Current-only FVCOM case without turbulence terms (for impact identification)
$n$	The number of records in the validation data	TEC	Tidal Energy Converter
$P$	The precipitation	TKE	Turbulent Kinetic Energy
$P_a$	The air pressure at sea surface	TSR	Tip Speed Ratio
$P_b$	The buoyancy production terms of turbulent kinetic energy		
$P_H$	The hydrostatic pressure		
$P_s$	The shear production terms of turbulent kinetic energy		

turn how these changes in flow affect the behaviours of the turbine itself.

Numerical oceanographic models (e.g., Regional Ocean Modelling System (ROMS) [13] and The Unstructured Grid Finite Volume Community Ocean Model (FVCOM) [14]) have also been used to study the far-field hydrodynamic changes caused by the operation of turbines and turbine arrays [15,16]. (Here, the far-field refers to the area in which the pressure distribution may be reasonably assumed linear). Such models must be modified in order to simulate the effect of tidal stream turbines. Such modifications found in the literature, overall, can be grouped into two different approaches: implementing an additional bottom friction on the seabed and modifying the flow motion with added turbine-induced forces. The first approach is often applied in two-dimensional studies [17–19]. However, it means the drag of the devices is exerted on the seabed, rather than in the water column, leading to unrealistic predicted effects. The second approach, known as ‘retarding force method’, as noted by Ref. [20], is generally more scientifically rigorous in comparison

with the ‘additional bottom friction’ method. Also, the extension of this concept to three dimensions is more logically feasible. Hence, the retarding force method is more widely applied in site-specific large scale impact assessment studies [21–27]. Unfortunately, these works largely relied on two-dimensional models, which is inconsistent with the physical meanings of the turbine representation methods. The two-dimensional models could also result in incomplete prediction of the vertical flow structure downstream of the turbine and hence the mixing in the wake [28,29]. In contrast, the vertical flow structure and the mixing in the wake of a turbine can be resolved in a three-dimensional model [26].

Another outstanding issue is that turbulent mixing downstream of the turbine has yet to become a major focus in large scale modelling. However, water flow within the near wake features a high turbulence level. Apart from the background turbulence, turbines introduce additional turbulence: flow accelerates and decelerates around blades, turbulent mixing occurs in the wake and interacts with the free stream [3], and mechanical turbulence

results from the rotating motion of the turbine [30]. It is reported in CFD simulation work that the original two-equation turbulence closure models are not sufficient to account for the extra Turbulent Kinetic Energy (TKE) production caused by turbines [30,31]. In an effort to account for this within ROMS [15], modified the  $k-\epsilon$  closure to simulate turbine-induced turbulence generation, dissipation and interference for the turbulence length-scale.

The primary objective of the work documented in this paper was to develop a Horizontal Axis Tidal Turbine (HATT) simulation system, that could simulate, on a realistic spatial scale, the impact of tidal stream turbines on flow speed and TKE in the far-field. This paper details the development of such a simulation system within the aforementioned three-dimensional oceanographic model—FVCOM. To represent the presence of the turbine and its operation, the current module within FVCOM is modified based on the ‘retarding force method’ and the turbulence module is modified based on simulation terms proposed by Ref. [15] for turbine-induced turbulence generation, dissipation and interference for the turbulence length-scale. A thorough validation study is also presented in which the developed model is tested, utilizing a combination of real experimental data collected from a prototype experiment conducted in the laboratory flume of [6], and CFD simulated results.

The structure of the paper is provided as follows for clarity. Firstly in Section 2 the FVCOM model is introduced and the integration of turbine simulation within this framework is discussed. Next, Section 3 details the validation study for the turbine which considers current and turbulence. Note that as the experimental data available was considered insufficient for comprehensive validation, this section also details generation of further validation data via CFD modelling (which itself was validated with the experimental data). In Section 4, the new model system is then applied to test cases in order to reveal impacts of a single turbine on the surroundings. Important results from Sections 3 and 4 are highlighted in Section 5 in terms of impact and potential future developments followed finally by concluding remarks in Section 6.

## 2. Modelling system

### 2.1. Three-dimensional FVCOM

FVCOM was selected to model the impacts of tidal stream energy devices on coastal regions. It is a three-dimensional, free surface, terrain-following oceanographic model for solving shallow water equations numerically using the finite-volume method [14]. There were three main considerations for choosing FVCOM as the basic modelling tool in the present work:

1. The model system includes fully coupled three-dimensional wave-current-sediment modules, which is critical for any realistic far-field modelling at a coastal regional scale.
2. It enables the use of an unstructured triangular mesh for discretisation of the computational domain, allowing for varied mesh resolution. Such a treatment of spatial discretisation is particularly important in this study as the mesh can be refined to particular high resolution around an individual turbine site and maintain a smooth transition to a relatively large mesh size far from the turbine so that the total computational cost can be restricted.
3. It provides a three-dimensional turbulence model ‘MY-2.5’ which is suitable for implementing the turbine effects at oceanographic scale simulations.

For completeness, the basic theory surrounding FVCOM is given in the following. More details of the model can be found in Ref. [32].

In Cartesian coordinates, the governing equations of FVCOM are:

$$\frac{\partial u}{\partial t} + u \frac{\partial u}{\partial x} + v \frac{\partial u}{\partial y} + w \frac{\partial u}{\partial z} - f v = -\frac{1}{\rho_0} \frac{\partial(P_H + P_a)}{\partial x} - \frac{1}{\rho_0} \frac{\partial q}{\partial x} + \frac{\partial}{\partial z} \left( K_m \frac{\partial u}{\partial z} \right) + F_u \quad (1)$$

$$\frac{\partial v}{\partial t} + u \frac{\partial v}{\partial x} + v \frac{\partial v}{\partial y} + w \frac{\partial v}{\partial z} + f u = -\frac{1}{\rho_0} \frac{\partial(P_H + P_a)}{\partial x} - \frac{1}{\rho_0} \frac{\partial q}{\partial y} + \frac{\partial}{\partial z} \left( K_m \frac{\partial v}{\partial z} \right) + F_v \quad (2)$$

$$\frac{\partial w}{\partial t} + u \frac{\partial w}{\partial x} + v \frac{\partial w}{\partial y} + w \frac{\partial w}{\partial z} = -\frac{1}{\rho_0} \frac{\partial q}{\partial z} + \frac{\partial}{\partial z} \left( K_m \frac{\partial w}{\partial z} \right) \quad (3)$$

$$\frac{\partial u}{\partial x} + \frac{\partial v}{\partial y} + \frac{\partial w}{\partial z} = 0 \quad (4)$$

where  $t$  is the time,  $x$ ,  $y$ , and  $z$  are the east, north, and vertical axes in the Cartesian coordinate system;  $u$ ,  $v$ , and  $w$  are the three velocity components in the  $x$ ,  $y$ , and  $z$  directions respectively;  $\rho_0$  is water density;  $P_a$  is the air pressure at sea surface;  $P_H$  is the hydrostatic pressure;  $q$  is the non-hydrostatic pressure;  $f$  is the Coriolis parameter and  $K_m$  is the vertical eddy viscosity coefficient.  $F_u$ ,  $F_v$  represent the additional horizontal momentum terms. In the present study, the turbine effects are represented through these two terms as specified in later section. The total water column depth is  $d = H + \zeta$ , where  $H$  is the bottom depth and  $\zeta$  is the height of the free surface.

The surface and bottom boundary conditions for  $u$ ,  $v$ , and  $w$  are:

$$K_m \left( \frac{\partial u}{\partial z}, \frac{\partial v}{\partial z} \right) = \frac{1}{\rho_0} (\tau_{sx}, \tau_{sy}), w = \frac{\partial \zeta}{\partial t} + u \frac{\partial \zeta}{\partial x} + v \frac{\partial \zeta}{\partial y} + \frac{E - P}{\rho}, \quad z = \zeta(x, y, t) \quad (5)$$

$$K_m \left( \frac{\partial u}{\partial z}, \frac{\partial v}{\partial z} \right) = \frac{1}{\rho_0} (\tau_{bx}, \tau_{by}), w = -u \frac{\partial H}{\partial x} - v \frac{\partial H}{\partial y}, \quad z = -H(x, y) \quad (6)$$

where  $(\tau_{sx}, \tau_{sy})$  and  $(\tau_{bx}, \tau_{by}) = C_d \sqrt{u^2 + v^2} (u, v)$  are the  $x$  and  $y$  components of surface wind and bottom stresses;  $E$  and  $P$  are evaporation and precipitation respectively. The drag coefficient  $C_d$  is determined by matching a logarithmic bottom layer to the model at a height  $z_{ab}$  above the bottom:

$$C_d = \max \left( \frac{\kappa^2}{\ln^2 \left( \frac{z_{ab}}{z_0} \right)}, 0.0025 \right) \quad (7)$$

where  $\kappa = 0.4$  is the von Karman constant and  $z_0$  is the bottom roughness parameter.

The three-dimensional MY-2.5 turbulence module is based on the following controlling equations:

$$\frac{\partial q^2}{\partial t} + u \frac{\partial q^2}{\partial x} + v \frac{\partial q^2}{\partial y} + w \frac{\partial q^2}{\partial z} = 2(P_s + P_b - \epsilon) + \frac{\partial}{\partial z} \left( K_q \frac{\partial q^2}{\partial z} \right) + F_q \quad (8)$$

$$\frac{\partial q^2 l}{\partial t} + u \frac{\partial q^2 l}{\partial x} + v \frac{\partial q^2 l}{\partial y} + w \frac{\partial q^2 l}{\partial z} = l E_1 \left( P_s + P_b - \frac{\bar{W}}{E_1} \varepsilon \right) + \frac{\partial}{\partial z} \left( K_q \frac{\partial q^2 l}{\partial z} \right) + F_l \quad (9)$$

where  $q^2 = (u^2 + v^2)/2$  is the turbulent kinetic energy;  $l$  is the macroscale;  $K_q$  is the vertical eddy diffusion coefficient of the turbulent kinetic energy;  $F_q$  and  $F_l$  represent the horizontal diffusion of the turbulent kinetic energy and macroscale;  $P_s = K_m(u_x^2 + v_x^2)$  and  $P_b = (gK_h \rho_z)/\rho_0$  are the shear and buoyancy production terms of turbulent kinetic energy;  $\varepsilon = q^3/B_1 l$  is the turbulent kinetic energy dissipation rate;  $B_1 = 16.60$  is a model coefficient;  $\bar{W} = 1 + E_2 l^2 / (\kappa L)^2$  is a wall proximity function where  $L^{-1} = (\zeta - z)^{-1} + (H + z)^{-1}$ ;  $E_1 = 1.80$  and  $E_2 = 1.33$  are model coefficients.  $F_q$  and  $F_l$  are parameterized using the Smagorinsky eddy parameterization method [33]. A constant value can also be assigned to the horizontal diffusion coefficient in FVCOM, which means the turbulence closure model can be run with both  $F_q$  and  $F_l$  set to zero.

The turbulent kinetic energy and macroscale equations are closed by defining:

$$K_m = l q S_m, \quad K_h = l q S_h, \quad K_q = 0.2 l q \quad (10)$$

where  $S_m$  and  $S_h$  are stability functions, calculation of which can be found in Ref. [32].

The surface and bottom boundary conditions for the turbulent kinetic energy and macroscale equations are:

$$q^2 l = 0, \quad q^2 = B_1^2 u_{\tau s}^2, \quad z = \zeta(x, y, t) \quad (11)$$

$$q^2 l = 0, \quad q^2 = B_1^2 u_{\tau b}^2, \quad z = -H(x, y) \quad (12)$$

where  $u_{\tau s}$  and  $u_{\tau b}$  are the water friction velocities associated with the surface and bottom. Since  $q^2 \neq 0$  at the surface and bottom,  $l = 0$  at both boundaries, which means  $K_m$ ,  $K_h$  and  $K_q$  are always 0 at the surface and bottom.

## 2.2. Representation of HATT in FVCOM

The original FVCOM is designed for ocean circulation in coupling with surface wave propagation at a regional scale. There is no direct tool available within the package to simulate tidal stream turbines. Therefore new features must be added into the model system to represent the turbine and its operation; these include changes to the current and turbulence modules.

### 2.2.1. Modelling HATT in current model

It is widely recognised that the deceleration of the passing flow, largely due to energy loss around the turbine as well as the blockage effect of the device, is the major impact of a turbine on its ambient current. In this work, the energy extraction process is modelled based on the additional sink term put forward by Ref. [21] as:

$$F_u = -C_{ext} \frac{1}{2} \rho_0 \cdot u \cdot |\vec{V}| \quad (13)$$

$$F_v = -C_{ext} \frac{1}{2} \rho_0 \cdot v \cdot |\vec{V}| \quad (14)$$

where  $F_u$  and  $F_v$  are the additional sink term components per unit area;  $C_{ext}$  is the energy extraction coefficient which determines the

strength of the sink term;  $\vec{V}$  is the flow velocity vector and  $|\vec{V}|$  is the magnitude of the velocity in a cell.

These two terms are added onto the right hand side of the horizontal momentum equations of FVCOM (Equations (1) and (2)) respectively. It should be noted that the purpose of these modifications are not to simulate detailed hydrodynamics immediately around each individual turbine blade, but to represent the modified flow field at 4D to 6D away from the turbine further downstream. The complex flow-turbine interactions in the immediate wake of the turbine violate the basic assumption in oceanographic models like FVCOM, i.e. the pressure distribution across water depth is linear, resulting in the exclusion of non-hydrostatic pressure terms. This particular difficulty means that the predictions from FVCOM are invalid in close proximity to the turbine. Although the distance at which the pressure distribution becomes linear will be dependent on the background turbulence level and configuration of the turbine, it has been observed by Ref. [3] to generally lie between 4D and 6D from the turbine disk. Therefore, the aim of the proposed modifications in the above-mentioned equations is to introduce accurate turbine effects to the passing flow beyond 4D-6D downstream of the device.

In addition, the present study identifies each individual turbine structure within a farm, rather than treating the entire turbine farm as a whole as in many previous studies [21,22,24,25]. In this way, the effects from each device can be identified. It is therefore proposed that the unstructured mesh is used with particularly fine resolution at each turbine device site. In the present study, mesh size close to the turbine is strictly assigned as the diameter of the device. To represent a turbine, an element of the model mesh is selected to exert the energy extraction coefficient ( $C_{ext}$ ) set along the water depth.  $C_{ext}$  of each sigma layer is treated individually in this research. Fig. 1 illustrates the turbine position in the x-y plane on the mesh, and Fig. 2 illustrates the three-dimensional application of the  $C_{ext}$  set. Layers between the two dotted lines are intercepted by the turbine. These layers are controlled by assigning  $C_{ext}$  values. Layers do not directly interact with the turbine are called 'free layers'.  $C_{ext}$  of these layers are 0. Such an approach is very different from previously mentioned two-dimensional studies [21–27] and a three-dimensional study [16] in which a single value was assigned to one of the layers, both of which failed to distinguish the velocity difference among various depths due to the turbine presence.

It should be noted that FVCOM is a mode-split model which calculates the velocity in both the two-dimensional external and three-dimensional internal modes. To ensure the consistency of the two modes, an adjustment is made in every internal time step to the three-dimensional internal mode, according to the results of the two-dimensional mode. Therefore, the sink term is also added into the two-dimensional external mode. The corresponding depth averaged  $C_{ext}$  is used in the two-dimensional mode. The effective velocity terms that account for the angle between the hub of the turbine and the flow direction proposed by Ref. [22] are not adopted in this research. Therefore, it is assumed that the turbine may yaw, allowing the rotor face to remain perpendicular to the incoming flow. Although this simplification is not representative of tidal turbines in general, efforts to introduce yaw controls that maximize effective rotor area are under-way e.g. Ref. [34]. Tidal turbines usually have an operational velocity window below which no power is generated and above which the power output is thresholded to the rated power output. The parameterization of this power limitation is discussed in detail in Ref. [23]. However, as the operating window is often application-specific, i.e., dependent on the type of turbine, and the present study focuses on generic representation of turbines in an oceanographic model system, the limit on power output is not accounted for.

2.2.2. Modelling HATT in turbulence model

The three turbine-induced turbulence perturbations identified in Ref. [15] are usually not accounted for in standard turbulence closures. In the present study however, each of the perturbations are represented following the terms proposed by Ref. [15] as follows:

- Turbine-induced turbulence generation,  $P_{tp}$

$$P_{tp} = C_{tp} \frac{u^3}{\Delta x} \tag{15}$$

- Turbine-induced turbulence dissipation,  $P_{td}$

$$P_{td} = C_{td} \frac{u \cdot k}{\Delta x} \tag{16}$$

- That of an interference for the turbulence length-scale ( $l$ ),  $P_l$

$$P_l = C_l \cdot P_s \tag{17}$$

$C_{tp}$ ,  $C_{td}$  and  $C_l$  in the aforementioned equations are coefficients decided empirically through parameter studies. The above mentioned terms are activated only at turbine locations.

With these three terms, Equations (8) and (9) become

$$\frac{\partial q^2}{\partial t} + u \frac{\partial q^2}{\partial x} + v \frac{\partial q^2}{\partial y} + w \frac{\partial q^2}{\partial z} = 2(P_s + P_b + P_{tp} - P_{td} - \epsilon) + \frac{\partial}{\partial z} \left( K_q \frac{\partial q^2}{\partial z} \right) + F_q \tag{18}$$

$$\frac{\partial q^2 l}{\partial t} + u \frac{\partial q^2 l}{\partial x} + v \frac{\partial q^2 l}{\partial y} + w \frac{\partial q^2 l}{\partial z} = l \left( E_1 (P_s + P_b) - P_l - \frac{\tilde{W}}{E_1} \epsilon \right) + \frac{\partial}{\partial z} \left( K_q \frac{\partial q^2 l}{\partial z} \right) + F_l \tag{19}$$

3. Model validation

3.1. Extending the available experimental data with a CFD model

Measurements from a laboratory experiment were available for the purpose of model validation. This experiment took place at the

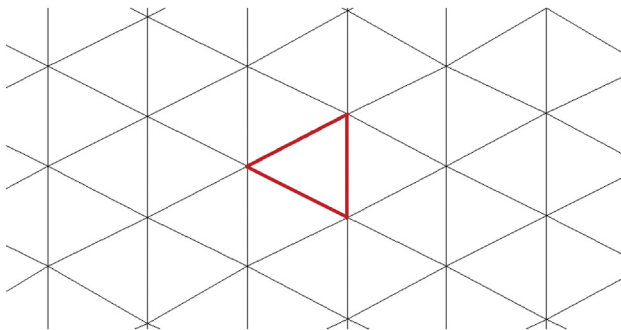


Fig. 1. Illustration of the turbine position in the x-y plane on the mesh. The red triangle indicates the mesh element in which the energy extraction coefficient set is exerted. (For interpretation of the references to colour in this figure legend, the reader is referred to the web version of this article.)

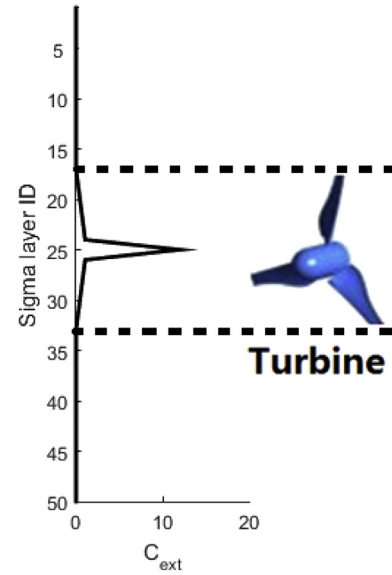


Fig. 2. Illustration of three-dimensional application of  $C_{ext}$  (see Equation (21)).

University of Hull using their ‘Environment Simulator Laboratory Flume’ [6]. The flume is 11 m in length, 1.6 m wide and 0.8 m deep (the water depth was 0.6 m). The inlet flow rate was 0.5 m/s. The diameter of the horizontal axis rotor used in this experiment was 200 mm and its hub was located 300 mm above the bed. The rotor was connected to a thick cylinder which was a part of the housing structure and the cylinder extended to about 1D downstream of the rotor. Tip speed ratio (TSR) of the rotor was 5.5. Measurements of velocity and TKE were taken along the centreline from 1D to 5D downstream of the rotor.

Although the experimental measurements cover a wide range of data that can be used for the present model validation purpose, they have apparent limitations. For example, the measured data only accounts for the distance down stream of the turbine up to 5D, which is not sufficient to reveal any effects beyond the point at which FVCOM is assumed valid. Therefore, to complement the experimental data, a CFD model based on ANSYS FLUENT (Version 14.5) is built to simulate the experimental conditions. The CFD model was first validated against the experimental measurements, then used to generate additional data for the FVCOM model validation.

FLUENT solves the three-dimensional Reynolds-Averaged Navier-Stokes (RANS) equations. Turbulence of the present research are calculated based on the Shear Stress Transport (SST)  $k-\omega$  model, following the conclusion of [35,36]. The Virtual Blade Model (VBM) is adopted in this research to simulate HATTs in FLUENT [37]. Essential configurations of VBM, i.e. geometrical setup and running parameters of the rotor, are specified according to [37].

3.2. CFD model validation

Fig. 3 shows a comparison of computed streamwise flow velocity against the measured experimental data. It can be seen that the velocity at the hub height 1D downstream of the rotor is 0 m/s which agrees with the observation in the laboratory, due to the supporting shaft. The velocity profiles at the other locations also match well with the laboratory data with root mean square error percentage ( $\%_{RMSE}$ ) of 14.3 at 3D, 18.4 at 4D and 20.8 at 5D (These values are also presented in Table 1). The  $\%_{RMSE}$  is calculated based on Equation (20) for each location. However, the model predicted velocity below the rotor is consistently slightly slower than the

measured data. This is likely due to a combination of underestimated bed friction and far proximity from the bed.

$$\%_{RMSE} = \frac{\sqrt{\frac{1}{n} \sum_{i=1}^n (q_i - q_{iest})^2}}{q_{max} - q_{min}} \times 100 \quad (20)$$

where  $n$  is the number of records in the validation data;  $q_i$  is the validation data;  $q_{iest}$  is the calculated result;  $q_{max}$  and  $q_{min}$  are the maximum and minimum records in the calculated result respectively.

The computed TKE results are compared with the measured data in Fig. 4. At 1D downstream of the rotor, the modelled data follows the measurements very well, including the maximum and minimum values of TKE around the rotor position. Further downstream at 3D, 4D and 5D, the model predicted TKE profile shapes agree with those measured in the laboratory ( $\%_{RMSE}$  refer to Table 1), i.e. the model is able to reproduce the enhanced turbulence at the rotor intercepted levels. The values at these levels, however, tend to be under-estimated by 15–20%. This is likely due to the CFD model not accounting for turbulence generated at the tip of rotor blades when in motion. Similar findings are reported in Ref. [31].

Overall, the agreement between FLUENT based CFD model results and measured data are considered to be satisfactory at all sites. The CFD predicted results within the rotor intersected region from 5D downstream can be used with confidence for FVCOM model validation.

### 3.3. Validation of the FVCOM model

With the validated CFD model available to complement the experimental data, it was possible to perform a thorough validation of the turbine simulation method developed within FVCOM. In the following, a number of validation tests are documented in which the FVCOM model is compared with the CFD model and where

**Table 1**  
 $\%_{RMSE}$  for the CFD case against the experimental data.

Velocity				TKE			
1D	3D	4D	5D	1D	3D	4D	5D
5.7	14.3	18.4	20.8	12.8	13.9	15.8	17.3

available, the original experimental data.

The FVCOM based model was firstly set up according to the experimental conditions mentioned above. The spatial resolution of the mesh is uniform in both stream-wise and cross-stream directions with a mesh size of 0.2 m (1D). Vertically, the water column is evenly divided into 50 sigma layers, this was found to provide a good trade-off between vertical resolution and simulation efficiency, i.e. it allows the evolving shapes of the velocity and TKE profiles over the water depth to be well captured without making the model computationally prohibitive. A uniform flow speed is achieved through maintaining a constant water level difference between the two ends of the channel.

As stated in Section 2, the turbine is represented by assigning  $C_{ext}$  values individually to the sigma layers. In this case, 17 out of 50 sigma layers are occupied by the turbine. The values of  $C_{ext}$  were decided through a process of iterative curve-fitting tests. Hence, the validation results presented represent the identified minimum  $\%_{RMSE}$  of these tests. The proposed approach was to have a vertically symmetrical linear increase over the layers occupied by the turbine, and a single dominating coefficient in the centre (see Equation (21)). This  $C_{ext}$  profile shape was determined empirically to produce velocity profiles that fitted well with the validation data. However, this definition of the  $C_{ext}$  profile shape may not be suitable in other applications and hence it is noted here that a wider study of possible profile shapes in general would be an interesting avenue for future research.

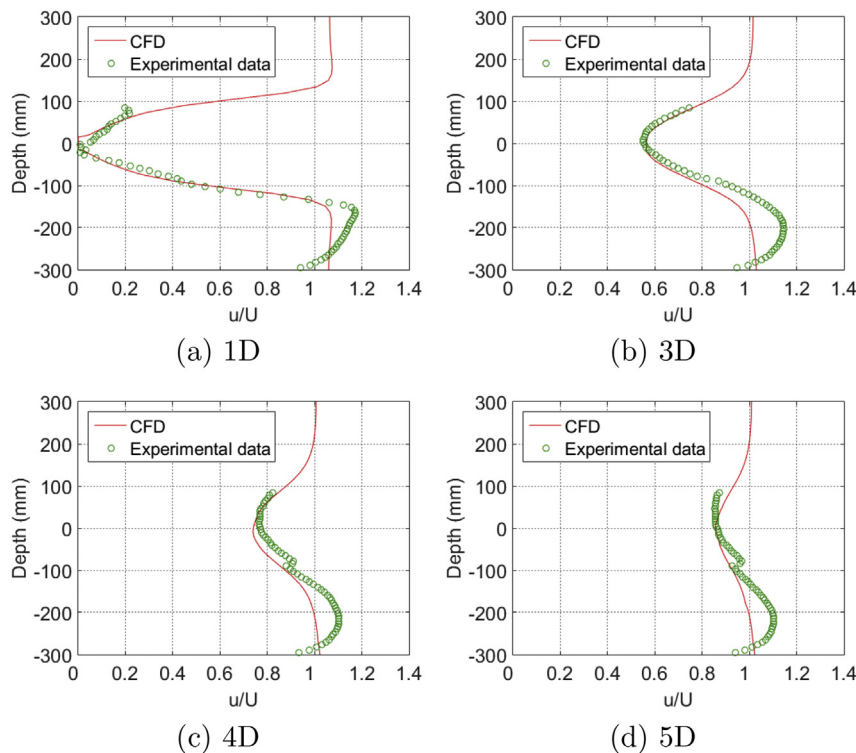


**Fig. 3.** Normalized velocity profiles of the CFD case against those measured in the laboratory at 1D, 3D, 4D and 5D downstream of the rotor.

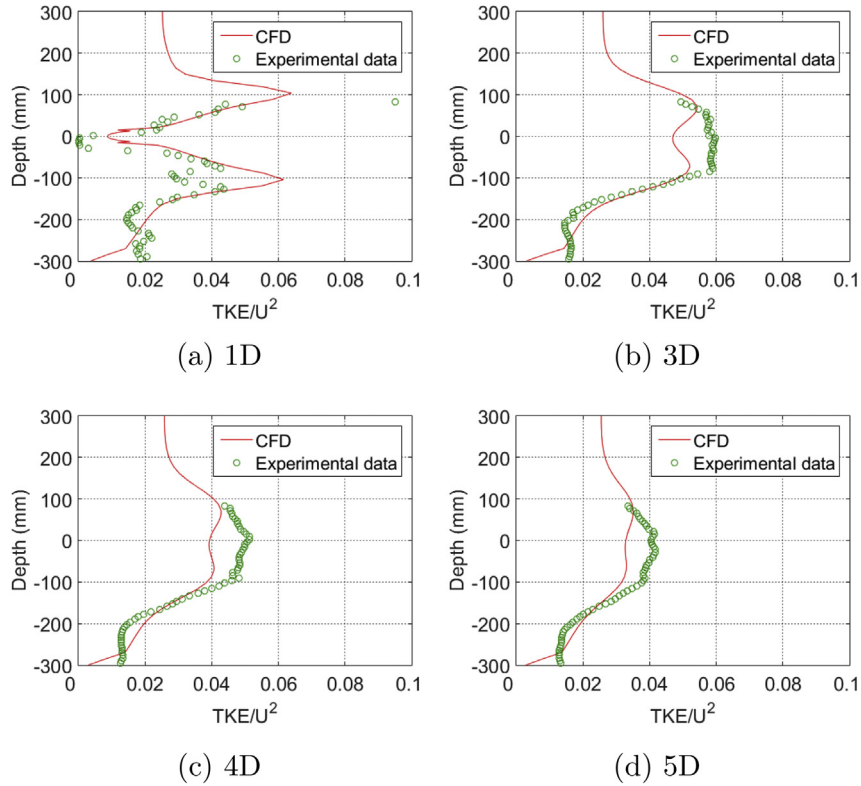


Fig. 4. Normalized TKE profiles of the CFD case against those measured in the laboratory at 1D, 3D, 4D and 5D downstream of the rotor.

$$C_{ext} = \begin{cases} m_1\sigma + c_1, & \sigma_{centre} > \sigma \geq \sigma_{min} \\ m_2\sigma + c_2, & \sigma_{max} > \sigma \geq \sigma_{centre} \\ C_{ext_{maxA}}, & \sigma = \sigma_{centre} \\ 0, & \text{otherwise} \end{cases} \quad (21)$$

where  $m_1 = C_{ext_{maxB}}/(\sigma_{centre} - \sigma_{min})$ ,  $m_2 = -m_1$ ,  $c_1 = -m_1\sigma_{min}$ ,  $c_2 = m_1\sigma_{max}$ , and  $\sigma_{max} = 2\sigma_{centre} - \sigma_{min}$ .  $C_{ext_{maxA}}$  is the dominant central coefficient,  $C_{ext_{maxB}}$  is the height of the  $C_{ext}$  profile not considering  $C_{ext_{maxA}}$  and  $\sigma_{min} < \sigma < \sigma_{max}$  is the domain covered by the rotor. The  $C_{ext}$  profile used in the current study is shown in Fig. 2. For completeness, the parameters introduced in Equation (21) used in this study are given in Table 2 along with coefficients to simulate impact of the turbine on the turbulence,  $C_{tp}$ ,  $C_{td}$  and  $C_l$ ; again, these are determined empirically based on the validation data. Finally, note that the depth-averaged value  $C_{ext}$  is 0.408.

To validate the FVCOM model, two cases are run for velocity and TKE validation: with and without the additional turbulence terms activated at the turbine location. These two cases are hereafter named TbM (with the terms) and TbO (without the terms).

Comparison of velocity profiles at 5D, 7D, 9D and 11D downstream of the turbine are shown in Fig. 5 (for % $_{RMSE}$  of these results refer to Table 3). This range is chosen due to the fact that up to 5D the model is highly likely to be invalid due to previously mentioned limitations of FVCOM, and beyond 11D there is little variation in the velocity profile. Within the turbine swept area, velocity profiles of both TbM and TbO show a satisfactory agreement with the experimental measurements at 5D. Slight under-prediction is observed in the near bed boundary layer, which is attributed to the under-predicted bed friction. Further downstream, there is significant overall agreement between the FVCOM and CFD predicted velocities, especially beyond 7D downstream of the turbine. Hence, the new model system is capable of predicting the far-wake of the

turbine correctly in terms of velocity, given appropriate  $C_{ext}$  values assigned. Beyond 9D downstream, both FVCOM and CFD model results show near uniform distributions of the velocity across the depth, indicating that the flow is less affected by both bottom and upper boundaries as well as the turbine operations in the far-wake.

Comparison of TKE profiles at 5D, 7D, 9D and 11D downstream of the turbine are shown in Fig. 6, again, for % $_{RMSE}$  of these results refer to Table 3. In Fig. 6 (a) case TbM predicted TKE matches better with the experimental data than the CFD model. This is due to the tendency of the CFD result to underestimate TKE levels as identified in Section 2. For this reason, it is assumed that at locations 7D and 9D where experimental data were not available, although case TbO more closely matches the CFD results, case TbM presents a more likely reflection of reality. Further, the differences in the computed TKE level between cases TbM and TbO become less significant as the wake recovers further downstream.

#### 4. Application—influence of turbulence closure terms

A series of tests are carried out in FVCOM to reveal impacts of a single turbine on the surroundings using a prototype 15 m diameter turbine model as the test bed. Water depth of these cases is 45 m and the turbine hub is located at a depth of 22.5 m. The flow conditions are set to reflect those of the Anglesey coast, North Wales, UK. This site is of particular interest for potential introduction of tidal turbine farms [38]. A water velocity of 1.0 m/s is defined, given

Table 2  
 $C_{ext}$  profile parameters and values of  $C_{tp}$ ,  $C_{td}$  and  $C_l$ .

$C_{ext_{maxA}}$	$C_{ext_{maxB}}$	$\sigma_{min}$	$\sigma_{centre}$	$C_{tp}$	$C_{td}$	$C_l$
12	1.2	17	25	0.08	0.1	2.8

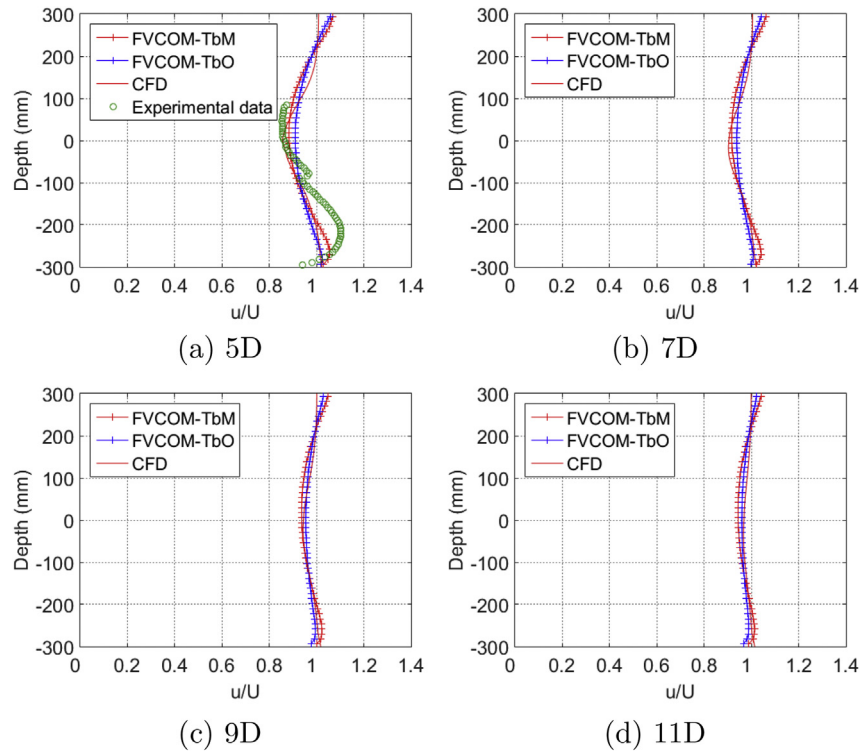


**Fig. 5.** Normalized velocity profiles of two FVCOM cases (with and without turbulence modification terms) against those predicted by the CFD case and measured in the laboratory at 5D, 7D, 9D and 11D downstream of the rotor.

by a time-average over one full tide cycle at the location [39]. These tests are conducted with and without the turbine implementations, i.e. the coefficients represent turbine effects being switched on and off, in order to reveal the differences between the baseline case (no turbine) and cases with turbine effects. Particular attention is given to the effects of enhanced turbulence.

Free-surface elevation, normalized depth-averaged velocity, water flow velocity in the bottom boundary layer and bed shear stress along the centreline are calculated under different scenarios: TbM15 (with turbulence terms), TbO15 (without turbulence terms) and undisturbed flow. These are shown in Fig. 7.

In Fig. 7, the turbine is placed at 0D and the horizontal axis shows distance in terms of turbine diameters (1D = 15 m). It can be seen that water level upstream of the turbine is higher than the undisturbed flow in both TbM15 and TbO15 (Fig. 7 (A)), accompanied by a substantial (~20%) drop of water velocity (Fig. 7 (B)). The passing flow is slowed down due to energy loss. The decelerated water accumulates in front of the turbine, causing the water level rise upstream of the turbine. Free-surface elevation drop is observed at the turbine location. The water level keeps dropping until 1D downstream of the turbine. These behaviours are consistent with measurements from a previously published laboratory experiment [7].

**Table 3**  
%RMSE for the four FVCOM cases.

Cases	Velocity				TKE			
	5D	7D	9D	11D	5D	7D	9D	11D
TbM	20.4	13.3	16.7	23.4	16.3	28.0	25.1	15.3
TbO	26.9	22.1	12.9	22.1	41.3	22.1	21.7	29.6

Errors at 5D are given against the experimental data; and against CFD results otherwise.

It is observed that only a very slight difference is caused by the turbulence closure terms to the calculated free surface elevation and depth-averaged velocity (<0.1% mean square difference between TbM15 and TbO15 in Fig. 7(A) and (B)). Also, both free surface elevation and depth-averaged velocity recover over a relatively short distance. Specifically, the depth-averaged velocity recovered to 96% of its original value within 2D downstream of the turbine for both TbM15 and TbO15 before recovery begins to stagnate. The recovery of surface water elevation also goes into stagnancy beyond 3D downstream the turbine. The water elevation is still slightly (~1%) below its undisturbed value at 25D downstream of the turbine. Similarly, depth-averaged velocity does not completely recover within a distance of 25D. Similar non-localized far-field impact is also reported in Ref. [40].

Changes incurred by the enhanced turbulent mixing (TbM15) to the flow velocity in the boundary layer and the bed shear stress, however, are obvious (Fig. 7 (C) & (D)). When compared to the undisturbed flow, the presence of the turbine increases the water velocity in the bottom layer, regardless of the turbulence calculation scheme. However, the increase is ~8% larger when the turbulence terms are activated (TbM15). Flow velocity and bed shear stress reach their maximum at roughly 1D downstream of the turbine. The downstream influential range of the turbine is beyond 25D for bottom layer water velocity and bottom shear stress in both TbM15 and TbO15. Further, it is important to note that a 2 N/m<sup>2</sup> increase in bottom shear stress beyond the undisturbed flow level can be seen in Fig. 7 (D) for TbM15, which exceeds the critical shear stress of medium sand, coarse sand and a range of fine gravel, as defined in Ref. [41]. This is mainly due to the accelerated flow near the bottom in the turbine wake. Increased bottom shear stress is also reported in laboratory work [6,42] as well as CFD simulations [37]. This is contrary to reduced bottom shear stress observations in previous two-dimensional studies [25,26], in which the bottom

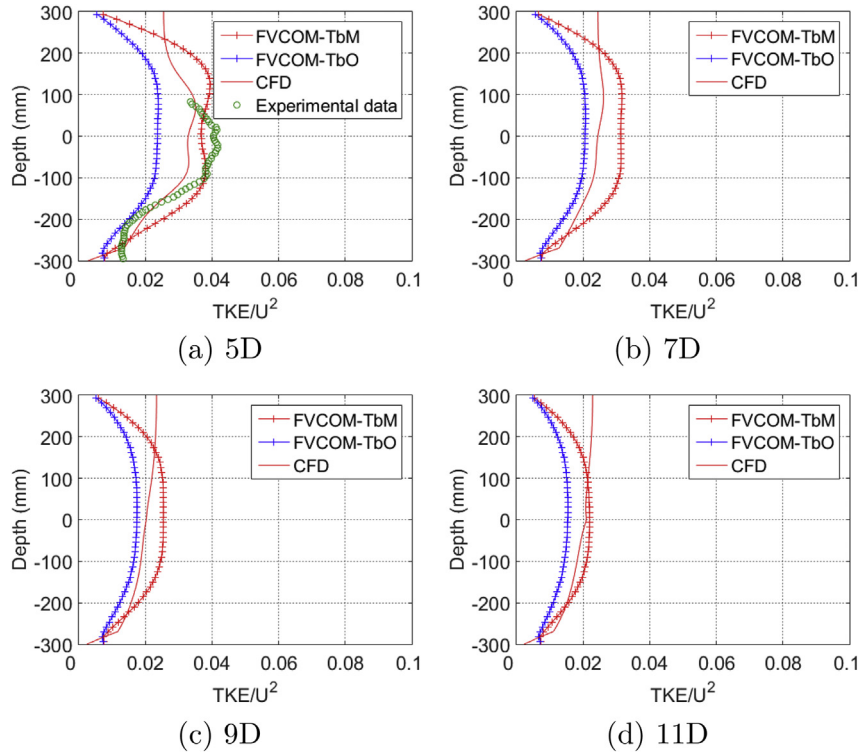


Fig. 6. Normalized TKE profiles of two FVCOM cases, TbM and TbO, against those predicted by the CFD case and measured in the laboratory at 5D, 7D, 9D and 11D downstream of the rotor.

shear stress is derived from reduced depth-averaged velocity. The bottom layer water velocity and bottom shear stress difference

caused by the turbulence calculation scheme starts to become negligible beyond 10D downstream of the turbine.

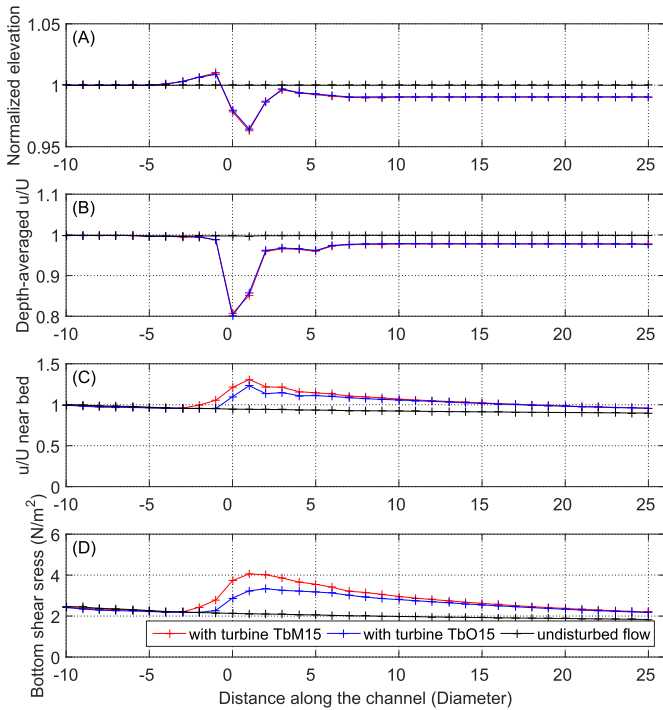


Fig. 7. (A) Normalized free-surface elevation (B) Normalized depth-averaged velocity (C) Normalized water velocity in the bottom layer and (D) Bottom shear stress along the centreline calculated under different scenarios: TbM15 - Retarding force + turbulence terms, TbO15 - Retarding force and undisturbed flow. (The turbine is positioned at 0D).

### 5. Discussion and research outlook

This study has highlighted the need of additional terms in the momentum equations and the turbulence closure (MY-2.5) of the three-dimensional FVCOM to simulate accurate hydrodynamics in the wake of turbines. The results demonstrate that an augmented FVCOM can produce satisfactory velocity and TKE profiles in the wake of a turbine (refer to Table 3 for comparison results of computed and measured profiles). However, one should note that in the current state of the proposed method, simulated wake still lacks rotational motion, which may result in inaccurate suspended sediment distribution.

Another important finding in this research is the increased bed shear stress predicted by the three-dimensional FVCOM, which agrees with results reported in physical experiment studies [6,42]. This is a result of the flow acceleration near the bed being identified by a three-dimensional model. This lies in contrast to a generally reduced flow in the wake predicted by a depth-averaged two-dimensional model, which commonly leads to bed stress weakening in the wake [25,26]. A precise prediction of bed shear stress is of particular importance, as it largely decides the sediment morphology [41].

Furthermore, it is noted that there is currently a gap in the literature on the implementation of effects of turbines on waves in large scale numerical modelling. However, small scale CFD simulations carried out by Ref. [37] showed that the wave height was reduced by roughly 17% and the wave length was increased by 19% due to the presence of a turbine rotor ( $D = 0.5$  m) with its hub located 0.39 m away from the free surface. Therefore, effects of turbines on surface waves are recommended as an important and

interesting avenue of investigation in future large scale numerical modelling studies in order to obtain a more complete simulation of tidal turbines. An introduction to this topic, presented by one of the authors can be found in Ref. [39].

## 6. Conclusions

In this study, a numerical model based on FVCOM for simulating far-field impacts of tidal turbines has been developed according to understandings obtained from laboratory measurements [6] and small scale CFD simulations. Apart from the widely acknowledged flow deceleration in the wake, TKE level in the wake was found to be increased due to the presence of turbines. Under-estimated TKE level predicted by small scale CFD and large scale FVCOM simulations without turbulence terms (case TbO) demonstrated the need of further treatment to the turbulence closures.

In more detail, to simulate the impact identified above in FVCOM, a body force was employed in the current module to account for the turbine-induced water deceleration. Three terms were added into the three-dimensional MY-2.5 turbulence closure to model turbine-related turbulence generation, dissipation and turbulence length-scale interference.

An idealized water channel was built to test the reliability of the developed turbine simulation system. The mesh resolution at the turbine location was set to the diameter of the prototype turbine used in the experiment so that turbines could be simulated individually. The validation results indicate that the three-dimensional retarding force method was able to address water velocity reduction effectively and correctly. The turbulence terms were shown to be necessary for accurate turbulent mixing prediction; without them being activated at the turbine location, under-prediction of TKE level behind the turbine was observed.

The standalone turbine tests demonstrated behaviours similar to those observed in a laboratory experiment [7] in terms of free surface elevation and depth-averaged velocity. The additional turbulence terms have little effect on the calculation of these two variables. An encouraging finding is that the enhanced bottom shear stress results were qualitatively consistent with laboratory observations. In reality, the increase in bottom shear stress is likely to be caused by the accelerated flow near the bottom as well as intensified mixing in the wake due to the turbine rotor in motion. These two processes could be simulated accurately in the present study due to the three-dimensional modelling system used.

To finalize, in this paper a numerical tool for impact assessment of large scale tidal turbine farms is presented. The turbine simulating platform is developed based on a three-dimensional large scale modelling system. When considering potential future work in the area of three-dimensional sediment transport modelling, the herein proposed treatment of flow velocity and turbulence level leading to accurate prediction of vertical flow structure and mixing in the wake of tidal turbines is of particular importance.

## Acknowledgement

X. Li would like to acknowledge support from the Chinese Scholar Council and the University of Liverpool. Dr. Sufian also provided the settings for VBM in ANSYS FLUENT. The authors are grateful to Brendan Murphy for his help setting-up and running the experiments. The authors would also like to acknowledge funding from the Engineering and Physical Sciences Research Council (EPSRC) to grant EP/J010359/1 (Interactions of flow, tidal stream turbines and local sediment bed under combined waves and tidal conditions), which is part of the Supergen consortium.

## References

- [1] F. Birol, et al., *World Energy Outlook*, Paris: International Energy Agency.
- [2] L. Myers, A. Bahaj, An experimental investigation simulating flow effects in first generation marine current energy converter arrays, *Renew. Energy* 37 (1) (2012) 28–36.
- [3] L. Myers, A. Bahaj, Experimental analysis of the flow field around horizontal axis tidal turbines by use of scale mesh disk rotor simulators, *Ocean Eng.* 37 (2) (2010) 218–227.
- [4] F. Maganga, G. Germain, J. King, G. Pinon, E. Rivoalen, Experimental characterisation of flow effects on marine current turbine behaviour and on its wake properties, *IET Renew. Power Gener.* 4 (6) (2010) 498–509.
- [5] S. Tedds, I. Owen, R. Poole, Near-wake characteristics of a model horizontal axis tidal stream turbine, *Renew. Energy* 63 (2014) 222–235.
- [6] L.B. Jordan, S. Simmons, S. McLelland, B. Murphy, D. Parsons, L. Vybulkova, The impact of tidal stream turbines on 3D flow and bed shear stress measured with particle image velocimetry in a laboratory flume, in: *Proceedings of the 11th European Wave and Tidal Energy Conference*, Nantes, France, 2015, pp. 654–660.
- [7] X. Sun, J. Chick, I. Bryden, Laboratory-scale simulation of energy extraction from tidal currents, *Renew. Energy* 33 (6) (2008) 1267–1274.
- [8] M. Harrison, W. Batten, L. Myers, A. Bahaj, Comparison between CFD simulations and experiments for predicting the far wake of horizontal axis tidal turbines, *IET Renew. Power Gener.* 4 (6) (2010) 613–627.
- [9] L. Bai, R.R. Spence, G. Dudziak, Investigation of the influence of array arrangement and spacing on tidal energy converter (TEC) performance using a 3-dimensional CFD model, in: *Proceedings of the 8th European Wave and Tidal Energy Conference*, Uppsala, Sweden, 2009, pp. 654–660.
- [10] X. Bai, E. Avital, A. Munjiza, J. Williams, Numerical simulation of a marine current turbine in free surface flow, *Renew. Energy* 63 (2014) 715–723.
- [11] R. Malki, I. Masters, A.J. Williams, T.N. Croft, Planning tidal stream turbine array layouts using a coupled blade element momentum–computational fluid dynamics model, *Renew. Energy* 63 (2014) 46–54.
- [12] A. Goude, O. Ågren, Simulations of a vertical axis turbine in a channel, *Renew. Energy* 63 (2014) 477–485.
- [13] A.F. Shchepetkin, J.C. McWilliams, The regional oceanic modeling system (ROMS): a split-explicit, free-surface, topography-following-coordinate oceanic model, *Ocean Model.* 9 (4) (2005) 347–404.
- [14] C. Chen, H. Liu, R.C. Beardsley, An unstructured grid, finite-volume, three-dimensional, primitive equations ocean model: application to coastal ocean and estuaries, *J. Atmos. Ocean. Technol.* 20 (1) (2003) 159–186.
- [15] T. Roc, D.C. Conley, D. Greaves, Methodology for tidal turbine representation in ocean circulation model, *Renew. Energy* 51 (2013) 448–464.
- [16] Z. Yang, T. Wang, A.E. Copping, Modeling tidal stream energy extraction and its effects on transport processes in a tidal channel and bay system using a three-dimensional coastal ocean model, *Renew. Energy* 50 (2013) 605–613.
- [17] I.G. Bryden, S.J. Couch, ME1 marine energy extraction: tidal resource analysis, *Renew. Energy* 31 (2) (2006) 133–139.
- [18] R. Karsten, J. McMillan, M. Lickley, R. Haynes, Assessment of tidal current energy in the Minas Passage, Bay of Fundy, *Proc. Inst. Mech. Eng. Part A J. Power Energy* 222 (5) (2008) 493–507.
- [19] I. Walkington, R. Burrows, Modelling tidal stream power potential, *Appl. Ocean Res.* 31 (4) (2009) 239–245.
- [20] S.J. Couch, I.G. Bryden, The impact of energy extraction on tidal flow development, in: *Proceedings of the 3rd International Conference on Marine Renewable Energy*, 2004.
- [21] Z. Defne, K.A. Haas, H.M. Fritz, Numerical modeling of tidal currents and the effects of power extraction on estuarine hydrodynamics along the Georgia coast, USA, *Renew. Energy* 36 (12) (2011) 3461–3471.
- [22] R. Ahmadian, R. Falconer, B. Bockelmann-Evans, Far-field modelling of the hydro-environmental impact of tidal stream turbines, *Renew. Energy* 38 (1) (2012) 107–116.
- [23] D.R. Plew, C.L. Stevens, Numerical modelling of the effect of turbines on currents in a tidal channel—Tory Channel, New Zealand, *Renew. Energy* 57 (2013) 269–282.
- [24] D. Fallon, M. Hartnett, A. Olbert, S. Nash, The effects of array configuration on the hydro-environmental impacts of tidal turbines, *Renew. Energy* 64 (2014) 10–25.
- [25] J. Thiébot, P.B. du Bois, S. Guillou, Numerical modeling of the effect of tidal stream turbines on the hydrodynamics and the sediment transport—application to the Alderney Race (Raz Blanchard), France, *Renew. Energy* 75 (2015) 356–365.
- [26] R. Martin-Short, J. Hill, S. Kramer, A. Avdis, P. Allison, M. Piggott, Tidal resource extraction in the Pentland Firth, UK: potential impacts on flow regime and sediment transport in the Inner Sound of Stroma, *Renew. Energy* 76 (2015) 596–607.
- [27] P.E. Robins, S.P. Neill, M.J. Lewis, Impact of tidal-stream arrays in relation to the natural variability of sedimentary processes, *Renew. Energy* 72 (2014) 311–321.
- [28] I. Bryden, S. Couch, A. Owen, G. Melville, Tidal current resource assessment, *Proc. Inst. Mech. Eng. Part A J. Power Energy* 221 (2) (2007) 125–135.
- [29] S. Serhadloglu, T.A. Adcock, G.T. Houlshby, S. Draper, A.G. Borthwick, Tidal stream energy resource assessment of the Anglesey Skerries, *Int. J. Mar. Energy* 3 (2013) e98–e111.

- [30] S.R. Turnock, A.B. Phillips, J. Banks, R. Nicholls-Lee, Modelling tidal current turbine wakes using a coupled RANS-BEMT approach as a tool for analysing power capture of arrays of turbines, *Ocean Eng.* 38 (11) (2011) 1300–1307.
- [31] M. Shives, C. Crawford, Adapted two-equation turbulence closures for actuator disk RANS simulations of wind & tidal turbine wakes, *Renew. Energy* 92 (2016) 273–292.
- [32] C. Chen, G. Cowles, R. Beardsley, An Unstructured Grid, Finite-volume Coastal Ocean Model: FVCOM User Manual, SMAST/UMASSD.
- [33] J. Smagorinsky, General circulation experiments with the primitive equations: I. the basic experiment, *Mon. Weather Rev.* 91 (3) (1963) 99–164.
- [34] C. Frost, C.E. Morris, A. Mason-Jones, D.M. O'Doherty, T. O'Doherty, The effect of tidal flow directionality on tidal turbine performance characteristics, *Renew. Energy* 78 (2015) 609–620.
- [35] R. McSherry, J. Grimwade, I. Jones, S. Mathias, A. Wells, A. Mateus, 3D CFD modelling of tidal turbine performance with validation against laboratory experiments, in: *Proceedings of the 9th European Wave and Tidal Energy Conference*, 2011.
- [36] G.I. Gretton, T. Bruce, D.M. Ingram, Hydrodynamic modelling of a vertical axis tidal current turbine using CFD, in: *Proceedings of the 8th European Wave and Tidal Energy Conference*, 2009, pp. 468–476.
- [37] S. Sufian, Numerical Modeling of Impacts from Horizontal axis Tidal Turbines, Ph.D. thesis, School of Engineering, University of Liverpool, 6 2016.
- [38] A. Iyer, S. Couch, G. Harrison, A. Wallace, Variability and phasing of tidal current energy around the United Kingdom, *Renew. Energy* 51 (2013) 343–357.
- [39] X. Li, 3D Modelling of Tidal Stream Energy Extraction for Impact Assessment, Ph.D. thesis, School of Engineering, University of Liverpool, 9 2016.
- [40] S.P. Neill, J.R. Jordan, S.J. Couch, Impact of tidal energy converter (tec) arrays on the dynamics of headland sand banks, *Renew. Energy* 37 (1) (2012) 387–397.
- [41] C. Berenbrock, A.W. Tranmer, Simulation of Flow, Sediment Transport, and Sediment Mobility of the Lower Coeur d'Alene River, Idaho, US Geological Survey, 2008.
- [42] C. Hill, M. Musa, L.P. Chamorro, C. Ellis, M. Guala, Local scour around a model hydrokinetic turbine in an erodible channel, *J. Hydraul. Eng.* 140 (8) (2014) 04014037.